Toroidal magnetic moments in Tb_4 squares†

Qianqian Yang,[a,b] Liviu Ungur, *[c] Wolfgang Wernsdorfer [d] and Jinkui Tang *[a,b]

Terbium-based complexes are passable in the study of single molecule toroics (SMTs). Herein, the syntheses and characterizations of a series of Tb_4 SMTs isolated from reduced or dimerized Schiff base ligands are presented. These complexes share a similar μ_4-O bridged Tb_4 square core and show diamagnetic ground states. Micro-SQUID technique was carried out on a single-crystal sample and the results suggest that there is a toroidal arrangement of the magnetic moments. *Ab initio* calculations are performed on these complexes and confirm the mixed-moment SMT properties. This allowed us to access a new strategy for generating single molecule toroics in terbium-based molecules.

Introduction

The toroidal magnetic moment is characterized by a vortex arrangement of magnetic dipoles $T = \sum_{i=1}^{N} r_i \times s_i$ ($N \geq 2$ spins per unit cell) and has long been discussed in the context of particle physics.[1] Due to the existence of ferrotoroidic order (Scheme 1, left),[2] this multi-spin object breaks both space inversion and time-reversal symmetries.[3] Therefore, the toroidal magnetic moment is regarded as a potential candidate for various applications, such as information storage, electronics, and magnetic and optical switches.[4] The recent search for the toroidal moment was mainly focused on metal-based materials in solid-state chemistry and physics, particularly the ferrotoroidic domains in $LiCoPO_4$.[3a,5] Since the seminal discovery of the non-magnetic ground state in Dy_3 triangular clusters in 2006, toroidal arrangement of magnetic moments have also been identified in single molecule based complexes,[6] namely single molecule toroics (SMTs), and have become a new class of magnetic materials.[4,7]

The typical feature of SMTs is a wheel-shaped topology, such as a Dy_3 triangle,[6,8] a Dy_4 square[7a,9] and a Dy_6 wheel,[10] in which the magnetic moments of the spin centers are in a vortex distribution and coupled through dipole and/or exchange interactions. Recently, SMT behaviors have also been extended to cubic topology Dy_4,[11] coupled Dy_3 [8b,12] and nanoscale cyclic coordination clusters.[13] However, most of the reported SMTs are dysprosium-based complexes, which is mainly because of the Kramer's nature and adaptable axial anisotropy in the vertebral coordination environment for the dysprosium ion.[14] The exploration of toroic behavior of molecules based on other elements is a new endeavor for the development of SMTs, but is very challenging.[15] Terbium possesses a similar oblate electron distribution as the dysprosium ion does, and also exhibits good or even better anisotropy and single molecule magnet (SMM) behavior.[16] For example, the first reported lanthanide-based SMM, $[Pc_2Ln]^-$, kept the record anisotropic energy for more than 10 years.[17] The recently reported single electron coupled Tb_2 inside fullerene shows a robust SMM property with a blocking temperature up to 28 K,[18] which is regarded as the best candidate for future applications.[19] However, in the research area of SMTs, a terbium-based complex is passable, and only a few examples

[a]*State Key Laboratory of Rare Earth Resource Utilization, Changchun Institute of Applied Chemistry, Chinese Academy of Sciences, Changchun 130022, PR China. E mail: tang@ciac.ac.cn*
[b]*School of Applied Chemistry and Engineering, University of Science and Technology of China, Hefei, Anhui 230026, PR China*
[c]*Department of Chemistry, National University of Singapore, 117543, Singapore. E mail: chmlu@nus.edu.sg*
[d]*Institute of Quantum Materials and Technologies, KIT, D 76344 Eggenstein Leopoldshafen, Germany*

†Electronic supplementary information (ESI) available: Experimental details and additional figures (Tables S1 S9 and Fig. S1 S20). CCDC 1487721 1487723. For ESI and crystallographic data in CIF or other electronic format see DOI: 10.1039/d1qi01459e

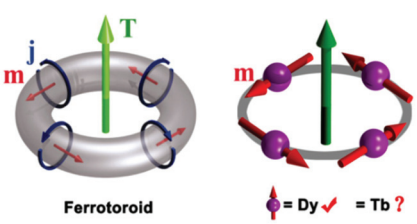

Scheme 1 Ring shaped solenoid with electric current loops as a clas sical example for a toroidal moment (left) and lanthanide based vortex type magnetic moment for a SMT (right). Copyright 2010 the American Association for the Advancement of Science.

have been reported showing a toroidal arrangement of the magnetic moments.[15,20]

In previous work, a Dy_4 square complex was obtained from a reduced bidentate Schiff base ligand H_3L^2, in which the multiple coordination environment facilitates the Dy^{III} ions to arrange the anisotropy axes in a toroidal fashion.[7a] In the research reported here, a similar terbium-based analog is synthesized to investigate the potential SMT behavior in this system. A novel tetranuclear complex, $[Tb_4(\mu_4\text{-OH})(HL^2)_4(NCS)_2]\cdot NCS\cdot CH_3CN\cdot 5CH_3OH$ (**1**), was isolated. In addition, using the relevant dimerized Schiff base ligands H_6L^3 (Scheme S1†) to modify the coordinate environment of the Tb^{III} ions, two isomorphic Tb_4 squares, namely $[Tb_4(\mu_4\text{-O})(H_2L^3)_2(NCS)_2]\cdot 6H_2O$ (**2**) and $[Tb_4(\mu_4\text{-O})(H_2L^3)_2Cl_2]\cdot 2CH_3CN\cdot 2H_2O\cdot 2CH_3OH$ (**3**) were obtained. Magnetic investigations suggest that these complexes possess diamagnetic ground states. Results from single-crystal micro-SQUID magnetometer measurements and *ab initio* calculations confirmed the diamagnetic ground states resulting from the toroidal arrangement of the magnetic moments.

Experimental

Materials and measurements

All reagents and solvents were commercially obtained and used as received without any further purification. The FT-IR spectra were measured using a Nicolet 6700 FT-IR spectrometer (ThermoFisher Scientific) equipped with a Smart iTR™ attenuated total reflectance (ATR) sampling accessory (ThermoFisher Scientific) in the range from 500 to 4000 cm^{-1}. Elemental analyses for C, H, N, and S were carried out on a 2400 CHNS organic element analyzer (PerkinElmer). Magnetic susceptibility measurements were performed on a MPMS XL7 SQUID magnetometer (Quantum Design) equipped with a 7 T magnet. The direct-current (dc) measurements were obtained in the temperature range of 1.9–300 K with an external magnetic field of 1000 Oe. Diamagnetic corrections were made using the Pascal's constants for all the constituent atoms as well as the contributions of the sample holder.[21]

Synthesis of H_3L^1. H_3L^1 was synthesized by the same procedure as described previously.[22] The condensation of 3-methoxysalicylaldehyde and 2-amino-2-methyl-1,3-propanediol in the molar ratio of 1 : 1 in 50 mL of ethanol at 80 °C for 12 h gave H_3L^1 as yellow powder. Yield: 92%. Selected IR (cm^{-1}): 3176.35 (br), 2999.94(w), 2904.66(w), 2839.63(w), 1637.22(s), 1604.98(s), 1543.54(m), 1493.99(s), 1442.01(m), 1393.77(w), 1369.34(w), 1339.11(w), 1217.02(s), 1159.77(m), 1063.38(s), 955.85(w), 925.41(m), 850.44(w), 778.52(w), 746.59(m), 719.59(w), 627.87(w).

Synthesis of ligand H_3L^2. Ligand H_3L^2 was obtained from H_3L^1 by reductive amination using $NaBH_4$ in dried methanol/dichloromethane.[23] Yield: 87%. Selected IR (cm^{-1}): 3342.65 (br), 2829.52(br), 1590.24(w), 1566.29(w), 1478.20(s), 1456.28(s), 1441.65(s), 1270.18(m), 1234.31(s), 1160.39(w), 1062.50(br), 887.63(w), 868.76(w), 846.31(w), 763.08(w), 729.49(m), 709.88()w1, 599.84(w).

Synthesis of ligand H_6L^3. Ligand H_6L^3 was synthesized by the same procedure as H_3L^1, using 1,3-bis(3-formyl-2-hydroxyphenoxy)propane to replace 3-methoxysalicylaldehyde.[23] Yield: 92%. Selected IR (cm^{-1}): 3249.86(br), 2921.68(br), 1626.95(s), 1608.35(s), 1510.28(s), 1468.10(m), 1347.22(w), 1224.15(s), 1166.24(m), 1140.55(m), 1044.12(m), 944.71(w), 911.00(w), 731.76(m), 622.36(w), 571.70(m).

Synthesis of complex 1. To a solution of $Tb(NCS)_3\cdot 6H_2O$ (0.2 mmol) and H_3L^2 (0.2 mmol) in 5 : 5 mL of methanol/acetonitrile, 0.4 mmol of triethylamine was added. The mixture was heated at 90 °C for 1 h, and then left undisturbed, and colorless crystals of **1** were produced after 2 d with a ~78% yield. Selected IR (cm^{-1}): 3504.08(br), 3220.59(br), 2952.53(br), 2836.82(w), 2723.04(w), 2059.64(vs), 1602.58(m), 1479.16(s), 1380.80(m), 1307.52(m), 1251.60(w), 1226.52(m), 1187.59(w), 1085.74(m), 1058.75(m), 1031.75(m), 983.53(w), 964.25(m), 889.04(w), 854.32(w), 817.68(w), 767.54(w), 719.33(w), 601.69(w). Anal. Calcd for $[Tb_4(\mu_4\text{-OH})(HL^2)_4(NCS)_2]\cdot NCS\cdot CH_3CN\cdot 5CH_3OH$ ($C_{58}H_{92}N_8O_{22}S_3Tb_4$, MW = 1985.25): C, 35.09%; H, 4.67%; N, 5.64%; S, 4.84%. Found: C, 34.87%; H, 4.52%; N, 5.53%; S, 5.02%.

Synthesis of complex 2. To a solution of $Tb(NCS)_3\cdot 6H_2O$ (0.2 mmol) and H_6L^3 (0.1 mmol) in 5 : 5 mL of methanol/acetonitrile, 0.4 mmol of triethylamine was added. The mixture was heated at 90 °C for 1 h, and then left undisturbed, and colorless crystals of **2** were produced after 2 d with a ~65% yield. Selected IR (cm^{-1}): 3504.08(br), 3307.37(br), 2925.53(br), 2832.96(w), 2723.04(w), 2048.06(vs), 1643.08(s), 1600.65(m), 1454.09(s), 1390.45(m), 1365.38(m), 1286.31(m), 1257.38(w), 1216.88(m), 1193.74(w), 1174.46(m), 1087.67(m), 1066.46(m), 1033.67(m), 991.26(w), 931.46(w), 860.11(w), 840.82(w), 817.68(w), 779.11(w), 730.90(w), 632.55(w), 615.19(w), 590.12(w), 574.69(w). Anal. Calcd for $[Tb_4(\mu_4\text{-O})(H_2L^3)_2(NCS)_2]\cdot 6H_2O$ ($C_{52}H_{72}N_6O_{23}S_2Tb_4$, MW = 1848.95): C, 33.78%; H, 3.93%; N, 4.55%; S, 3.47%. Found: C, 34.01%; H, 3.82%; N, 4.59%; S, 3.62%.

Synthesis of complex 3. The same procedure was employed to synthesize complex **3** with $Tb(NCS)_3\cdot 6H_2O$ being replaced by $TbCl_3\cdot 6H_2O$. Yield: 54%. Selected IR (cm^{-1}) for **3**: 3334.37(br), 3191.66(br), 2927.46(w), 2840.68(w), 2751.97(w), 1645.01(s), 1602.58(m), 1456.01(s), 1390.45(m), 1286.31(s), 1222.67(s), 1197.60(m), 1174.46(m), 1085.74(m), 1066.46(m), 1031.75(m), 989.32(m), 929.54(m), 862.04(w), 819.61(w), 777.18(w), 730.90(m), 634.48(w), 613.26(w), 590.12(w). Anal. Calcd for $[Tb_4(\mu_4\text{-O})(H_2L^3)_2Cl_2]\cdot 2CH_3CN\cdot 2H_2O\cdot 2CH_3OH$ ($C_{56}H_{78}Cl_2N_6O_{21}Tb_4$, MW = 1877.82): C, 35.82%; H, 4.19%; N, 4.48%. Found: C, 35.70%; H, 4.20%; N, 4.41%.

Crystallography

Single-crystal X-ray data of the title complexes were collected on an Apex II CCD diffractometer (Bruker) equipped with graphite-monochromatized Mo-Kα radiation (λ = 0.71073 Å) at 273(2) K. The structures were solved by direct methods and refined by full-matrix least-squares methods on F^2 using SHELXTL-2014.[24] All non-hydrogen atoms were determined from the difference Fourier maps and refined anisotropically.

Hydrogen atoms were introduced in calculated positions and refined with fixed geometry with respect to their carrier atoms. Crystallographic data are listed in Table S1 (ESI).† CCDC 1487721–1487723† contains the supplementary crystallographic data for this research.

Results and discussion

Single-crystal X-ray studies revealed that complex **1** crystallizes in a triclinic space group *P*1 (Table S1, ESI†). The structure is centrosymmetric and contains two molecules (Fig. S1, ESI†). The two molecules are isostructural and each is constituted by one μ_4-OH bridge, four Tb^{III} ions, four ligands, two coordinated SCN^-, and one free SCN^- in the lattice. The μ_4-OH^- bridge resides in the center of the molecule and binds the four Tb^{III} ions in the same plane, forming a Tb_4 square. Two ligands cover the top of the square, and the other two lie under the bottom, sandwiching the Tb_4 square. Two coordinated SCN^- were attached to the Tb^{III} ions at the terminal sides. The orientations of the coordinated SCN^- in the two molecules were different: in molecule **a**, the SCN^- is almost in line with Tb–N direction (Tb–N–C angle of 174.86°), whereas in molecule **b**, the SCN^- is off to the Tb–N direction with a Tb–N–C angle of 152.67° (Fig. S1, ESI†). The ligands on the same side are parallel, whereas on the bifacial side they are antiparallel. As a result, the Tb^{III} ions are in different coordination environments: Tb1 is eight coordinated and resides at the joint point of the two ligands, and Tb2 is nine coordinated and resides at the crossing corner of the bifacial ligands. The structure core possesses one positive charge, which is balanced by one free SCN^- anion in the lattice.

Complexes **2** and **3** were obtained from the reaction of a terbium salt with a dimerized shift base ligand H_6L^3. The structures show similar Tb_4 square topology with a μ_4-O^{2-} bridge binding four Tb^{III} ions (Fig. 1). Two ligands reside on the top and bottom sides of the square, sandwiching the Tb_4 plane, which is similar to complex **1**. Due to the conjunction of the two Schiff-base units, the coordination pockets on the ligand are much closer, and as a result, the Tb_4 square is compressed along Tb2–Tb2′ direction with a relatively shorter Tb2–Tb2′ distance than that in complex **1** (Table S2, ESI†). In complex **2**, the ligands are slightly twisted, and the NCS^- coordinates with Tb1 to balance the positive charge. In complex **3**, the Cl^- coordinates with Tb1 to balance the charge (Fig. 1).

Although the structures of complexes **1–3** are similar, the small differences on the ligand and counterions probably influence the coordinate geometry and magnetic properties significantly. To investigate these effects, the coordinate geometries of **1–3** were calculated using SHAPE 2.1 software.[25] In complex **1**, the Tb^{III} ions are in a similar coordination environment with Tb1 close to biaugmented trigonal prism (C_{2v}) with a continuous shape measure (CShM) value of 2.19 for molecule **a** and 2.15 for molecule **b**. The Tb2 is close to the tricapped trigonal prism (D_{3h}) with CShM values of 0.78 and 0.73 for molecules **a** and **b**, respectively, (Table S3, ESI†). The situation for **3** is similar, where the Tb1 is close to the biaugmented trigonal prism (C_{2v}) with a CShM value of 2.79, Tb2 is close to the tricapped trigonal prism (D_{3h}) with a CShM value of 0.93 (Table S3, ESI†). Whereas for complex **2**, the coordination geometries are closer to a triangular dodecahedron (D_{2d}) with a CShM value of 2.42 for Tb1 and a capped square antiprism (C_{4v}) with a CShM value of 0.96 for Tb2. The distances between the two neighboring Tb^{III} ions are in the range of 3.53–3.58 Å, suggesting possible magnetic coupling between the Tb^{III} ions (see next section).

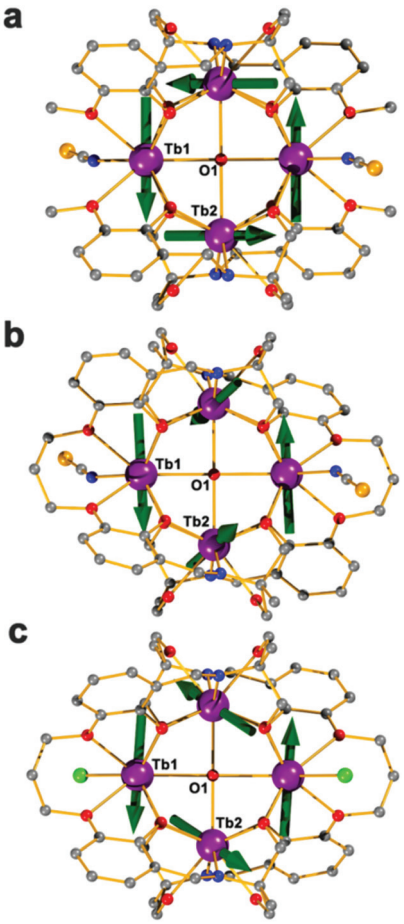

Fig. 1 Structures of the molecule **a** in complex **1** (a), complexes **2** (b) and **3** (c) with the green vectors representing the orientations of the main magnetic axes of the Tb^{III} ions. Purple, dark gray, blue, red, green, and orange spheres represent Tb, C, N, O, Cl, and S, respectively. Hydrogen atoms and solvents have been omitted for clarity.

The dc magnetic susceptibility measurements were performed on polycrystalline samples of complexes **1–3** in the temperature range 2–300 K under a 1 kOe dc field (Fig. 2). At room temperature, the $\chi_M T$ (χ_M = molar magnetic susceptibility) products for complexes **1–3** are 47.23, 46.08, and 46.74 $cm^3\ K\ mol^{-1}$, respectively, which were in good agreement with the free-ion approximation of four Tb^{III} ions (47.28 $cm^3\ K\ mol^{-1}$). Upon cooling, the $\chi_M T$ values decreased slowly until 25 K, and then dropped sharply, reaching the minimal values of 4.81, 8.57, and 6.55 $cm^3\ K\ mol^{-1}$ at 2 K, for complexes **1**, **2**,

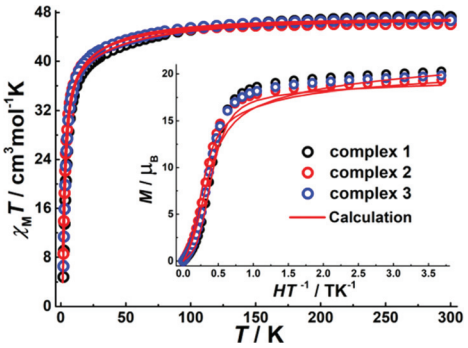

Fig. 2 The temperature dependence of the $\chi_M T$ products at 1 kOe between 2 and 300 K for **1** (black), **2** (red), and **3** (blue). The inset shows the plots of magnetization *M versus H*/*T* for **1–3** at 1.9 K. The red lines represent the results from *ab initio* calculations.

and **3**, respectively. The sharp drop and small $\chi_M T$ products at low temperatures probably indicate the existence of dominant antiferromagnetic interactions or a toroidal arrangement of the magnetic moments.

To investigate the low-temperature magnetism of these complexes, field-dependent molar magnetization (M) measurements were carried out on the polycrystalline samples at low temperatures (Fig. S4–S6, ESI†). The *M versus H* and H/T plots for complexes **1–3** at 1.9 K (Fig. 2 inset) show a slow increase at low magnetic fields and then a fast increase at about 5 kOe, which indicates the diamagnetic ground states of these complexes. This effect is very significant for measurements in the range of −2 to 2 T at 1.9 K (Fig. 3).

The micro-SQUID technique was carried out on a single crystal sample of **1** to further investigate the diamagnetic ground states. The normalized magnetization *versus H* plot shows a linear increase at 5 K (Fig. S7, ESI†). Upon cooling, a plateau is observed around the zero field below 2 K, which is in good agreement with the plot for the polycrystalline samples. The plateau is much more significant below 0.5 K with a steep appearance at 5.5 kOe. Then the magnetization at 0.5 K was measured with variable sweep rates of the magnetic field. Narrow openings of the hysteresis loops were observed between −5 and 5 kOe around the zero field (Fig. S8, ESI†), which was expected for SMM behavior. Upon further cooling to 0.03 K, the openings were much wider with a value of $0.015M_s$, indicating the mixed-moment SMT behavior (Fig. 4). The differential of the normalized magnetization of $d(M/M_s)/dH$ under different temperatures shows clear maxima with a crossing field H_c = ±6.4 and 0 kOe (Fig. S9, ESI†), which indicates that quantum tunneling occurs at these fields. The quantum tunneling of magnetization probably corresponds to the crossings of the magnetic states under the Zeeman splitting effect.[26]

To gain further insight into the magnetic anisotropy of the molecule, *ab initio* calculations were performed on these complexes based on their X-ray determined structure. Mononuclear Tb^{III} fragments were also included in the calculation of the CASSCF/RASSI/SINGLE ANISO types with the MOLCAS 8.0 software,[27] in which all the other three Tb^{III} ions were computationally substituted with diamagnetic Lu^{III} ions. As shown in Table S4 (ESI),† the ground doublet states of each Tb^{III} ion were well separated from the excited states with large g_z of more than 16. The energy gap between the ground doublet and the first excited state was larger than 26.59 cm^{-1} for each Tb^{III} ion. However, these complexes did not show relaxation of magnetization in the ac measurements, which is probably because of the non-Kramers nature of the Tb^{III} ions that facilitated the relaxation by the quantum tunneling processes. The axes of the magnetic moments between two neighboring Tb^{III} ions in molecules **a** and **b** of complex **1** were orthogonal with angles of 89.40° and 89.32°, suggesting the presence of toroidal magnetic moments (Fig. 1 and S14, ESI†), which was in good agreement with the Micro-SQUID measurements. For complexes **2** and **3**, the relevant angles were relatively small (71.16° and 67.63°). The dihedral angle between the planes formed by the magnetic axes of the two opposite sites in complexes **2** (62.51°, Fig. S15, ESI†) and **3** (41.03°, Fig. S16, ESI†) was larger than that in **1** (26.09° for molecule **a** and 23.28° for molecule **b**). This lead to a relatively smaller excitation energy from the ground non-magnetic (toroidal) state to the magnetic states (excited) in **2** and **3**, compared to

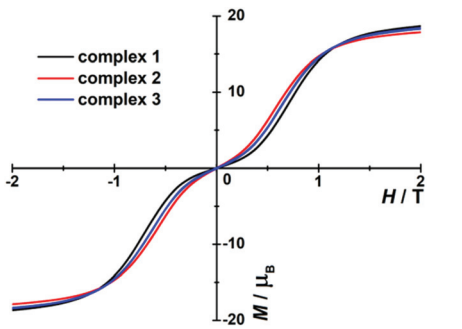

Fig. 3 Molar magnetization *M versus H* for polycrystalline samples of **1** (black), **2** (red), and **3** (blue) at 1.9 K.

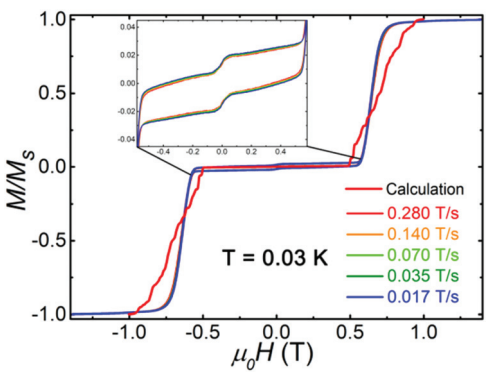

Fig. 4 The M/M_s at 0.03 K with the indicated dc field sweep rate for a single crystalline sample of complex **1**. The red line represents the calculated molar magnetization for molecule **a** in **1**. Inset: zoomed in plots in the magnetic field range of 0.58 to 0.58 T.

1, which indicated that **1** had a better SMT property. The relatively large magnetic susceptibility at 1.9 K in the dc measurements (*vide supra*) describes this difference well. The magnetic interaction is described as a sum of magnetic exchange and dipole–dipole magnetic contributions. All the crystal field states with energies below 100 cm^{-1} were included in the exchange mixing. The magnetic exchange is considered within the Lines model, whereas the dipole–dipole interaction is accounted for exactly, using the on-side magnetic moments obtained in the fragment calculations (eqn (S1)–(S3), ESI†). The parameters of the magnetic exchange interactions are adjusted to describe the measured magnetic properties. These calculations were done with the POLY ANISO code. The best-fitted values of the magnetic exchange are given in Table S5 (ESI).† The energies obtained for the exchange and dipolar interactions are given in Tables S6–S9 (ESI),† whereas the comparison between the measured and calculated magnetism is shown in Fig. S17–S20 (ESI).† The agreement between measured and calculated magnetism is rather high. Regardless of this difference in magnetic exchange values, the energy gap between the ground non-magnetic and the first excited state is similar. The calculated molar magnetization at T = 0.03 K for molecule **a** in **1** also fits the micro-SQUID measurements well (Fig. 4), which confirms that the diamagnetic ground states are from the toroidal arrangement of the magnetic moments of the Tb^{III} ions.

Conclusions

Three μ_4-O^{2-} bridged Tb_4 squares were successfully assembled by employing the reduced and dimerized Schiff-base ligands. Magnetic susceptibility measurements for both polycrystalline and single-crystal samples suggest that these complexes show typical single molecule toroic (SMT) behavior benefitting from the compressed axial coordinate environment and the strong intramolecular interactions. The *ab initio* calculations confirmed the toroidal arrangement of the magnetic moment and the magnetic couplings. These results highlight a promising strategy for generating single molecule toroics in terbium-based molecules.

Conflicts of interest

There are no conflicts to declare.

Acknowledgements

The authors thank the Key Research Program of Frontier Sciences, CAS (ZDBS-LY-SLH023), the Key Research Program of the Chinese Academy of Sciences (ZDRW-CN-2021-3-3) and the National Natural Science Foundation of China (21871247) for financial support. JT gratefully acknowledges the support of the Royal Society for a Newton Advanced Fellowship (NA160075). LU acknowledges financial support from the National University of Singapore research projects (R-143-000-A65-133 and R-143-000-A80-114). The *Ab initio* calculations were performed on the ASPIRE-1 cluster at the National Supercomputer Centre, Singapore (http://www.nscc.sg, project 11001278).

Notes and references

1 (*a*) V. M. Dubovik and V. V. Tugushev, Toroid moments in electrodynamics and solid-state physics, *Phys. Rep.*, 1990, **187**, 145–202; (*b*) F. Manfred, Revival of the magnetoelectric effect, *J. Phys. D: Appl. Phys.*, 2005, **38**, R123; (*c*) B. B. Van Aken, J.-P. Rivera, H. Schmid and M. Fiebig, Observation of ferrotoroidic domains, *Nature*, 2007, **449**, 702–705.

2 T. Kaelberer, V. A. Fedotov, N. Papasimakis, D. P. Tsai and N. I. Zheludev, Toroidal Dipolar Response in a Metamaterial, *Science*, 2010, **330**, 1510–1512.

3 (*a*) A. S. Nicola, F. Manfred and M. Maxim, The toroidal moment in condensed-matter physics and its relation to the magnetoelectric effect, *J. Phys.: Condens. Matter*, 2008, **20**, 434203; (*b*) C. Ederer, Toroidal moments as indicator for magneto-electric coupling: the case of $BiFeO_3$ versus $FeTiO_3$, *Eur. Phys. J. B*, 2009, **71**, 349–354; (*c*) K. M. Rabe, Solid-state physics: Response with a twist, *Nature*, 2007, **449**, 674–675.

4 L. Ungur, S.-Y. Lin, J. Tang and L. F. Chibotaru, Single-molecule toroics in Ising-type lanthanide molecular clusters, *Chem. Soc. Rev.*, 2014, **43**, 6894–6905.

5 (*a*) C. Ederer and N. A. Spaldin, Towards a microscopic theory of toroidal moments in bulk periodic crystals, *Phys. Rev. B: Condens. Matter Mater. Phys.*, 2007, **76**, 214404; (*b*) A. S. Zimmermann, D. Meier and M. Fiebig, Ferroic nature of magnetic toroidal order, *Nat. Commun.*, 2014, **5**, 4796.

6 J. Tang, I. Hewitt, N. T. Madhu, G. Chastanet, W. Wernsdorfer, C. E. Anson, C. Benelli, R. Sessoli and A. K. Powell, Dysprosium Triangles Showing Single-Molecule Magnet Behavior of Thermally Excited Spin States, *Angew. Chem., Int. Ed.*, 2006, **45**, 1729–1733.

7 (*a*) C. Das, S. Vaidya, T. Gupta, J. M. Frost, M. Righi, E. K. Brechin, M. Affronte, G. Rajaraman and M. Shanmugam, Single-Molecule Magnetism, Enhanced Magnetocaloric Effect, and Toroidal Magnetic Moments in a Family of Ln4 Squares, *Chem. – Eur. J.*, 2015, **21**, 15639–15650; (*b*) X.-L. Li and J. Tang, Recent developments in single-molecule toroics, *Dalton Trans.*, 2019, **48**, 15358–15370.

8 (*a*) I. J. Hewitt, J. Tang, N. T. Madhu, C. E. Anson, Y. Lan, J. Luzon, M. Etienne, R. Sessoli and A. K. Powel, Coupling Dy_3 Triangles Enhances Their Slow Magnetic Relaxation, *Angew. Chem., Int. Ed.*, 2010, **49**, 6352–6356; (*b*) S.-Y. Lin, W. Wernsdorfer, L. Ungur, A. K. Powell, Y.-N. Guo, J. Tang, L. Zhao, L. F. Chibotaru and H.-J. Zhang, Coupling Dy_3 Triangles to Maximize the Toroidal Moment, *Angew. Chem., Int. Ed.*, 2012, **51**, 12767–12771; (*c*) X.-L. Li, J. Wu, J. Tang,

B. Le Guennic, W. Shi and P. Cheng, A planar triangular Dy_3 + Dy_3 single-molecule magnet with a toroidal magnetic moment, *Chem. Commun.*, 2016, **52**, 9570–9573; (*d*) G. Novitchi, G. Pilet, L. Ungur, V. V. Moshchalkov, W. Wernsdorfer, L. F. Chibotaru, D. Luneau and A. K. Powell, Heterometallic Cu^{II}/Dy^{III} 1D chiral polymers: chirogenesis and exchange coupling of toroidal moments in trinuclear Dy_3 single molecule magnets, *Chem. Sci.*, 2012, **3**, 1169–1176; (*e*) S. Xue, X.-H. Chen, L. Zhao, Y.-N. Guo and J. Tang, Two Bulky-Decorated Triangular Dysprosium Aggregates Conserving Vortex-Spin Structure, *Inorg. Chem.*, 2012, **51**, 13264–13270; (*f*) Y.-X. Wang, W. Shi, H. Li, Y. Song, L. Fang, Y. Lan, A. K. Powell, W. Wernsdorfer, L. Ungur, L. F. Chibotaru, M. Shen and P. Cheng, A single-molecule magnet assembly exhibiting a dielectric transition at 470 K, *Chem. Sci.*, 2012, **3**, 3366–3370; (*g*) M. Gysler, F. El Hallak, L. Ungur, R. Marx, M. Hakl, P. Neugebauer, Y. Rechkemmer, Y. Lan, I. Sheikin, M. Orlita, C. E. Anson, A. K. Powell, R. Sessoli, L. F. Chibotaru and J. van Slageren, Multitechnique investigation of Dy_3 - implications for coupled lanthanide clusters, *Chem. Sci.*, 2016, **7**, 4347–4354; (*h*) R. Sessoli, M.-E. Boulon, A. Caneschi, M. Mannini, L. Poggini, F. Wilhelm and A. Rogalev, Strong magneto-chiral dichroism in a paramagnetic molecular helix observed by hard X-rays, *Nat. Phys.*, 2015, **11**, 69–74; (*i*) J. Luzon, K. Bernot, I. J. Hewitt, C. E. Anson, A. K. Powell and R. Sessoli, Spin Chirality in a Molecular Dysprosium Triangle: The Archetype of the Noncollinear Ising Model, *Phys. Rev. Lett.*, 2008, **100**, 247205; (*j*) L. Zhong, W.-B. Chen, Z.-J. OuYang, M. Yang, Y.-Q. Zhang, S. Gao, M. Schulze, W. Wernsdorfer and W. Dong, Unprecedented one-dimensional chain and two-dimensional network dysprosium(III) single-molecule toroics with white-light emission, *Chem. Commun.*, 2020, **56**, 2590–2593.

9 P.-H. Guo, J.-L. Liu, Z.-M. Zhang, L. Ungur, L. F. Chibotaru, J.-D. Leng, F.-S. Guo and M.-L. Tong, The First $\{Dy_4\}$ Single-Molecule Magnet with a Toroidal Magnetic Moment in the Ground State, *Inorg. Chem.*, 2012, **51**, 1233–1235.

10 (*a*) S.-Y. Lin, Y.-N. Guo, G.-F. Xu and J. Tang, Research Progress on Pure Lanthanide Single-Molecule Magnets, *Chin. J. Appl. Chem.*, 2010, **27**, 1365–1371; (*b*) A. Baniodeh, N. Magnani, S. Brase, C. E. Anson and A. K. Powell, Ligand field variations: tuning the toroidal moment of Dy_6 rings, *Dalton Trans.*, 2015, **44**, 6343–6347; (*c*) L. Ungur, S. K. Langley, T. N. Hooper, B. Moubaraki, E. K. Brechin, K. S. Murray and L. F. Chibotaru, Net Toroidal Magnetic Moment in the Ground State of a $\{Dy_6\}$-Triethanolamine Ring, *J. Am. Chem. Soc.*, 2012, **134**, 18554–18557; (*d*) S. K. Langley, B. Moubaraki, C. M. Forsyth, I. A. Gass and K. S. Murray, Structure and magnetism of new lanthanide 6-wheel compounds utilizing triethanolamine as a stabilizing ligand, *Dalton Trans.*, 2010, **39**, 1705–1708; (*e*) J. Wu, L. Zhao, L. Zhang, X.-L. Li, M. Guo, A. K. Powell and J. Tang, Macroscopic Hexagonal Tubes of 3d–4f Metallocycles, *Angew. Chem., Int. Ed.*, 2016, **55**, 15574–15578; (*f*) J. Wu, X.-L. Li, M. Guo, L. Zhao, Y. Zhang and J. Tang, Realization of toroidal magnetic moments in heterometallic 3d-4f metallocycles, *Chem. Commun.*, 2018, **54**, 1065–1068.

11 G. Fernandez Garcia, D. Guettas, V. Montigaud, P. Larini, R. Sessoli, F. Totti, O. Cador, G. Pilet and B. Le Guennic, A Dy_4 Cubane: A New Member in the Single-Molecule Toroics Family, *Angew. Chem., Int. Ed.*, 2018, **57**, 17089–17093.

12 (*a*) K. R. Vignesh, S. K. Langley, A. Swain, B. Moubaraki, M. Damjanović, W. Wernsdorfer, G. Rajaraman and K. S. Murray, Slow Magnetic Relaxation and Single-Molecule Toroidal Behaviour in a Family of Heptanuclear $\{Cr^{III}Ln^{III}_6\}$ (Ln=Tb, Ho, Er) Complexes, *Angew. Chem., Int. Ed.*, 2018, **57**, 779–784; (*b*) K. R. Vignesh, A. Soncini, S. K. Langley, W. Wernsdorfer, K. S. Murray and G. Rajaraman, Ferrotoroidic ground state in a heterometallic $\{Cr^{III}Dy^{III}_6\}$ complex displaying slow magnetic relaxation, *Nat. Commun.*, 2017, **8**, 1023.

13 (*a*) H.-L. Zhang, Y.-Q. Zhai, L. Qin, L. Ungur, H. Nojiri and Y.-Z. Zheng, Single-Molecule Toroic Design through Magnetic Exchange Coupling, *Matter*, 2020, **2**, 1481–1493; (*b*) H. Kaemmerer, A. Baniodeh, Y. Peng, E. Moreno-Pineda, M. Schulze, C. E. Anson, W. Wernsdorfer, J. Schnack and A. K. Powell, Inorganic Approach to Stabilizing Nanoscale Toroidicity in a Tetraicosanuclear $Fe_{18}Dy_6$ Single Molecule Magnet, *J. Am. Chem. Soc.*, 2020, **142**, 14838–14842.

14 (*a*) O. Kahn, *Molecular magnetism*, VCH, 1993; (*b*) P. Zhang and J. Tang, *Lanthanide Single Molecule Magnets*, Springer-Verlag, 2015; (*c*) D. Gatteschi, Anisotropic dysprosium, *Nat. Chem.*, 2011, **3**, 830–830.

15 (*a*) S. K. Langley, K. R. Vignesh, T. Gupta, C. J. Gartshore, G. Rajaraman, C. M. Forsyth and K. S. Murray, New examples of triangular terbium(III) and holmium(III) and hexagonal dysprosium(III) single molecule toroics, *Dalton Trans.*, 2019, **48**, 15657–15667; (*b*) S. K. Langley, K. R. Vignesh, B. Moubaraki, G. Rajaraman and K. S. Murray, Oblate versus Prolate Electron Density of Lanthanide Ions: A Design Criterion for Engineering Toroidal Moments? A Case Study on $\{Ln^{III}_6\}$ (Ln=Tb, Dy, Ho and Er) Wheels, *Chem. – Eur. J.*, 2019, **25**, 4156–4165.

16 (*a*) J. M. Clemente-Juan, E. Coronado and A. Gaita-Arino, Magnetic polyoxometalates: from molecular magnetism to molecular spintronics and quantum computing, *Chem. Soc. Rev.*, 2012, **41**, 7464–7478; (*b*) J. D. Rinehart and J. R. Long, Exploiting single-ion anisotropy in the design of f-element single-molecule magnets, *Chem. Sci.*, 2011, **2**, 2078–2085.

17 (*a*) M. Perfetti, M. Serri, L. Poggini, M. Mannini, D. Rovai, P. Sainctavit, S. Heutz and R. Sessoli, Molecular Order in Buried Layers of $TbPc_2$ Single-Molecule Magnets Detected by Torque Magnetometry, *Adv. Mater.*, 2016, **28**, 6946–6951; (*b*) C. Wäckerlin, F. Donati, A. Singha, R. Baltic, S. Rusponi, K. Diller, F. Patthey, M. Pivetta, Y. Lan, S. Klyatskaya, M. Ruben, H. Brune and J. Dreiser, Giant Hysteresis of Single-Molecule Magnets Adsorbed on a Nonmagnetic

Insulator, *Adv. Mater.*, 2016, **28**, 5195–5199; (*c*) N. Ishikawa, M. Sugita and W. Wernsdorfer, Quantum Tunneling of Magnetization in Lanthanide Single-Molecule Magnets: Bis(phthalocyaninato)terbium and Bis(phthalocyaninato)dysprosium Anions, *Angew. Chem., Int. Ed.*, 2005, **44**, 2931–2935; (*d*) A. Lodi Rizzini, C. Krull, T. Balashov, J. J. Kavich, A. Mugarza, P. S. Miedema, P. K. Thakur, V. Sessi, S. Klyatskaya, M. Ruben, S. Stepanow and P. Gambardella, Coupling Single Molecule Magnets to Ferromagnetic Substrates, *Phys. Rev. Lett.*, 2011, **107**, 177205; (*e*) S. Thiele, F. Balestro, R. Ballou, S. Klyatskaya, M. Ruben and W. Wernsdorfer, Electrically driven nuclear spin resonance in single-molecule magnets, *Science*, 2014, **344**, 1135–1138; (*f*) C. R. Ganivet, B. Ballesteros, G. de la Torre, J. M. Clemente-Juan, E. Coronado and T. Torres, Influence of peripheral substitution on the magnetic behavior of single-ion magnets based on homo- and heteroleptic Tb(III) bis(phthalocyaninate), *Chem. – Eur. J.*, 2013, **19**, 1457–1465.

18 (*a*) J. D. Rinehart, M. Fang, W. J. Evans and J. R. Long, A N_2^{3-} Radical-Bridged Terbium Complex Exhibiting Magnetic Hysteresis at 14 K, *J. Am. Chem. Soc.*, 2011, **133**, 14236–14239; (*b*) F. Liu, D. S. Krylov, L. Spree, S. M. Avdoshenko, N. A. Samoylova, M. Rosenkranz, A. Kostanyan, T. Greber, A. U. B. Wolter, B. Büchner and A. A. Popov, Single molecule magnet with an unpaired electron trapped between two lanthanide ions inside a fullerene, *Nat. Commun.*, 2017, **8**, 16098; (*c*) F. Liu, G. Velkos, D. S. Krylov, L. Spree, M. Zalibera, R. Ray, N. A. Samoylova, C.-H. Chen, M. Rosenkranz, S. Schiemenz, F. Ziegs, K. Nenkov, A. Kostanyan, T. Greber, A. U. B. Wolter, M. Richter, B. Büchner, S. M. Avdoshenko and A. A. Popov, Air-stable redox-active nanomagnets with lanthanide spins radical-bridged by a metal–metal bond, *Nat. Commun.*, 2019, **10**, 571; (*d*) F. Liu, L. Spree, D. S. Krylov, G. Velkos, S. M. Avdoshenko and A. A. Popov, Single-Electron Lanthanide-Lanthanide Bonds Inside Fullerenes toward Robust Redox-Active Molecular Magnets, *Acc. Chem. Res.*, 2019, **52**, 2981–2993; (*e*) G. Velkos, D. S. Krylov, K. Kirkpatrick, L. Spree, V. Dubrovin, B. Büchner, S. M. Avdoshenko, V. Bezmelnitsyn, S. Davis, P. Faust, J. Duchamp, H. C. Dorn and A. A. Popov, High Blocking Temperature of Magnetization and Giant Coercivity in the Azafullerene $Tb_2@C_{79}N$ with a Single-Electron Terbium–Terbium Bond, *Angew. Chem., Int. Ed.*, 2019, **58**, 5891–5896; (*f*) Y. Wang, G. Velkos, N. J. Israel, M. Rosenkranz, B. Büchner, F. Liu and A. A. Popov, Electrophilic Trifluoromethylation of Dimetallofullerene Anions en Route to Air-Stable Single-Molecule Magnets with High Blocking Temperature of Magnetization, *J. Am. Chem. Soc.*, 2021, **143**, 18139–18149.

19 (*a*) F. Paschke, T. Birk, V. Enenkel, F. Liu, V. Romankov, J. Dreiser, A. A. Popov and M. Fonin, Exceptionally High Blocking Temperature of 17 K in a Surface-Supported Molecular Magnet, *Adv. Mater.*, 2021, **33**, 2102844; (*b*) L. Spree, F. Liu, V. Neu, M. Rosenkranz, G. Velkos, Y. Wang, S. Schiemenz, J. Dreiser, P. Gargiani, M. Valvidares, C.-H. Chen, B. Büchner, S. M. Avdoshenko and A. A. Popov, Robust Single Molecule Magnet Monolayers on Graphene and Graphite with Magnetic Hysteresis up to 28 K, *Adv. Funct. Mater.*, 2021, **31**, 2105516.

20 (*a*) S. Biswas, S. Das, T. Gupta, S. K. Singh, M. Pissas, G. Rajaraman and V. Chandrasekhar, Observation of Slow Relaxation and Single-Molecule Toroidal Behavior in a Family of Butterfly-Shaped Ln_4 Complexes, *Chem. – Eur. J.*, 2016, **22**, 18532–18550; (*b*) S. Biswas, P. Kumar, A. Swain, T. Gupta, P. Kalita, S. Kundu, G. Rajaraman and V. Chandrasekhar, Phosphonate-assisted tetranuclear lanthanide assemblies: observation of the toroidic ground state in the Tb^{III} analogue, *Dalton Trans.*, 2019, **48**, 6421–6434.

21 E. A. Boudreaux and L. N. Mulay, *Theory and Applications of Molecular Paramagnetism*, John Wiley & Sons, New York, 1976.

22 (*a*) P. Zhang, L. Zhang, S.-Y. Lin and J. Tang, Tetranuclear $[MDy]_2$ compounds and their dinuclear [MDy] (M = Zn/Cu) building units: their assembly, structures, and magnetic properties, *Inorg. Chem.*, 2013, **52**, 6595–6602; (*b*) L. Zhao, J. Wu, H. Ke and J. Tang, Family of Defect-Dicubane Ni_4Ln_2 (Ln = Gd, Tb, Dy, Ho) and Ni_4Y_2 Complexes: Rare Tb(III) and Ho(III) Examples Showing SMM Behavior, *Inorg. Chem.*, 2014, **53**, 3519–3525.

23 J. Wu, S.-Y. Lin, S. Shen, X.-L. Li, L. Zhao, L. Zhang and J. Tang, Probing the Magnetic Relaxation and Magnetic Moments Arrangement in a Series of Dy_4 Squares, *Dalton Trans.*, 2017, **46**, 1577–1584.

24 (*a*) G. M. Sheldrick, A short history of SHELX, *Acta Crystallogr., Sect. A: Found. Crystallogr.*, 2008, **64**, 112–122; (*b*) XPREP, *Space Group Determination and Reciprocal Space Plots*, Siemens Analytical X-ray Instruments, Madison, WI, 1991.

25 D. Casanova, P. Alemany, J. M. Bofill and S. Alvarez, Shape and Symmetry of Heptacoordinate Transition-Metal Complexes: Structural Trends, *Chem. – Eur. J.*, 2003, **9**, 1281–1295.

26 (*a*) S.-G. Wu, Z.-Y. Ruan, G.-Z. Huang, J.-Y. Zheng, V. Vieru, G. Taran, J. Wang, Y.-C. Chen, J.-L. Liu, L. T. A. Ho, L. F. Chibotaru, W. Wernsdorfer, X.-M. Chen and M.-L. Tong, Field-induced oscillation of magnetization blocking barrier in a holmium metallacrown single-molecule magnet, *Chem*, 2021, **7**, 982–992; (*b*) Y.-C. Chen, J.-L. Liu, W. Wernsdorfer, D. Liu, L. F. Chibotaru, X.-M. Chen and M.-L. Tong, Hyperfine-Interaction-Driven Suppression of Quantum Tunneling at Zero Field in a Holmium(III) Single-Ion Magnet, *Angew. Chem., Int. Ed.*, 2017, **56**, 4996–5000.

27 (*a*) F. Aquilante, J. Autschbach, A. Baiardi, S. Battaglia, V. A. Borin, L. F. Chibotaru, I. Conti, L. D. Vico, M. Delcey, I. F. Galván, N. Ferré, L. Freitag, M. Garavelli, X. Gong, S. Knecht, E. D. Larsson, R. Lindh, M. Lundberg, P. Å. Malmqvist, A. Nenov, J. Norell, M. Odelius, M. Olivucci, T. B. Pedersen, L. Pedraza-González,

Q. M. Phung, K. Pierloot, M. Reiher, I. Schapiro, J. Segarra-Martí, F. Segatta, L. Seijo, S. Sen, D.-C. Sergentu, C. J. Stein, L. Ungur, M. Vacher, A. Valentini and V. Veryazov, Modern quantum chemistry with [Open]Molcas, *J. Chem. Phys.*, 2020, **152**, 214117; (*b*) G. Karlström, R. Lindh, P.-Å. Malmqvist, B. O. Roos, U. Ryde, V. Veryazov, P.-O. Widmark, M. Cossi, B. Schimmelpfennig, P. Neogrady and L. Seijo, MOLCAS: a program package for computational chemistry, *Comput. Mater. Sci.*, 2003, **28**, 222–239; (*c*) F. Aquilante, L. De Vico, N. Ferré, G. Ghigo, P.-å. Malmqvist, P. Neogrády, T. B. Pedersen, M. Pitoňák, M. Reiher, B. O. Roos, L. Serrano-Andrés, M. Urban, V. Veryazov and R. Lindh, MOLCAS 7: The Next Generation, *J. Comput. Chem.*, 2010, **31**, 224–247.